

Optical design for a survey x-ray telescope

Timo T. Saha^a, William W. Zhang^a, and Ryan S. McClelland^b

^aNASA/Goddard Space Flight Center, 8800 Greenbelt Road, Greenbelt, MD 20771

^bSGT, Inc, 7701 Greenbelt Road Suite 400, Greenbelt MD 20770

ABSTRACT

Optical design trades are underway at the Goddard Space Flight Center to define a telescope for an x-ray survey mission. Top-level science objectives of the mission include the study of x-ray transients, surveying and long-term monitoring of compact objects in nearby galaxies, as well as both deep and wide-field x-ray surveys. In this paper we consider Wolter, Wolter-Schwarzschild, and modified Wolter-Schwarzschild telescope designs as basic building blocks for the tightly nested survey telescope. Design principles and dominating aberrations of individual telescopes and nested telescopes are discussed and we compare the off-axis optical performance at 1.0 KeV and 4.0 KeV across a 1.0-degree full field-of-view.

Keywords: Optical design, x-ray optics, x-ray mirrors, wide-field x-ray telescopes

1. INTRODUCTION

X-ray grazing incidence telescopes are not well suited for wide-field applications. Depending on the energy range and coating selection, the reflection efficiency is rapidly lost if the grazing angles are larger than 0.5 to 2.0 degrees. Typically the field-of-view is limited to 1.0-degrees. Figure 1 illustrates a type 1 telescope. The Wolter (W) type 1 [1] telescope is the most common grazing incidence telescope used in x-ray astrophysics applications. These designs consist of a paraboloidal primary mirror followed by a confocal hyperboloidal secondary mirror. Transverse ray aberration expansions have been developed for all combinations of W-telescopes [2, 3]. In case of W type 1 telescopes, the third order coma and the curvature of the best focal surface are the dominating aberrations. Curvature of the best focal surface includes both third and fifth order aberration terms. In fact, seventh order aberration terms need to be taken into account in case of W type 1 telescopes.

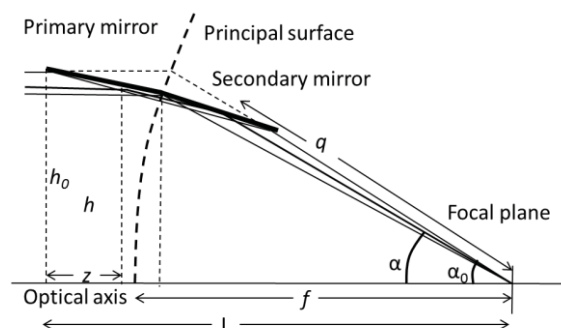


Figure 1. Drawing of type 1 telescope showing optical components, focal plane, principal surface, and extreme rays reflecting from the surfaces.

Wolter-Schwarzschild (WS) [4] telescopes provide a clear improvement over W-telescopes in terms of off-axis performance. WS-designs satisfy Abbe's sine condition and therefore, are free of lowest order coma aberration. At a Gaussian focal plane the images of a point source produced by WS-telescopes are typically round tori and nearly symmetric, indicating that field curvature is the dominating aberration. In case of W-telescope, the off-axis images are typically double circles [2] indicating presence of coma and field curvature in the system. At the best focal surface, the effects of field curvature aberration terms are minimized and the image of WS-telescope collapses to a smaller image which has higher order aberrations, but the image is still quite symmetric. At the best focal surface of W-telescope the coma aberration remains and the images show typical double-circles of coma minimized so that the circles are about the same size. The ray density is largest at a point where the coma circles intersect and, thus, the image is not very symmetric. The best focal surface of W- and WS-telescopes is nearly quadratic and the same. This is because the main aberration terms generating the field curvature are directly proportional to the square of the field angle.

The off-axis image sizes of WS-telescopes can be especially improved at the best focal surface by adding a small amount of second order axial sag to the primary or secondary mirror of the WS-telescope. We call these designs Modified-Wolter-Schwarzschild (MWS) telescopes.

In solar x-ray applications large field-of-views (1.0 - 1.25 degrees) are desirable. Thompson [5] designed a hyperboloid-hyperboloid telescope using an optimizer of a commercial ray tracing software. He achieved significantly improved off-axis image quality at the expense of on-axis and near on-axis image quality. This process effectively balanced the aberrations across the field-of-view. This design is a grazing incidence equivalent of Ritchie-Chretien normal incidence telescope design where the hyperboloids are used to minimize the third order coma.

Burrows [6] introduced polynomial grazing incidence telescopes. In this concept the optimization capabilities of modern optical design software are used to solve for the coefficients of the surface equations, expressed as the first few radial terms of a power series. Since then, Conconi [6], Elsner [7], and Roming [8] have used similar techniques to design type 1 grazing incidence polynomial telescopes for wide field applications.

In order to increase the effective area of x-ray telescopes, several mirror pairs need to be nested inside each other. Nesting of individual telescopes typically decreases the telescope off-axis performance partially because focal lengths of the nested individual telescopes do not match and are not perfectly aligned. The aberrations of individual telescopes cause image defects and lead to separations between the off-axis images produced by the telescopes. Also, the best focal surfaces of the individual telescopes do not match mainly because of the aberrations that change the field curvature aberration terms.

In this paper we compare imaging capabilities of individual W-, WS-, MWS-telescopes in terms of Half Power Diameter (HPD). We show the design principles and underlying surface equations of W- and WS-telescopes and also present the design principles underlying the MWS-telescopes. We also present the design principles for the nested telescopes and show how to minimize the off-axis image size and maximize the effective area of the nested telescopes. Finally, we present and analyze single mirror-pair designs and nested designs for wide-field W-, WS-, and MWS-telescopes and compare their optical performance.

2. SURFACE EQUATIONS OF WOLTER AND WOLTER-SCHWARZSCHILD TELESCOPES

Surface equations of W- and WS-telescopes can be combined into two sets of equations, one equation for the primary mirrors and the second equation for the secondary mirrors. The surface equations are a complex parametric set of equations expressed in terms of the telescope physical length, focal length, and maximum radial height at the entrance aperture. Figures 1 and 2 list the parameters and show the overall geometry. WS-telescopes satisfy the Abbe's sine condition which means that the radial height of the primary mirror can be expressed as a function of the focal length and back angle α of the secondary mirror:

$$h = f \sin(\alpha). \quad (1)$$

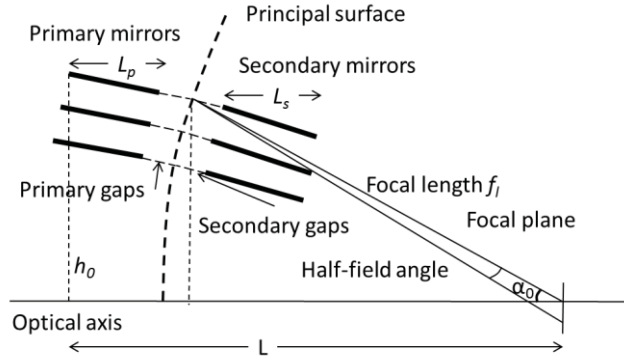


Figure 2. Cross-section of nested telescope showing the mirror locations and parameters used in the designs.

Equation (1) simply means that variables h and α define a circle with a radius of the focal length f . This circle is the principal surface of the telescope. The extensions of the ray after reflections from the surfaces intersect on the principal surface as illustrated in Figure 1. W-telescope consists of a parabolic primary mirror and confocal hyperbolic secondary mirror. Parameters h and α of the W-telescopes are related through an equation:

$$h = 2ft \tan\left(\frac{\alpha}{2}\right) = 2ft. \quad (2)$$

Equation (2) indicates that the variables h and α define a parabolic surface with an axial radius of curvature f [10]. This means that the principal surface of W-telescopes is parabolic. This shape of the principal surface is responsible for the coma aberration in W-telescopes. Equations (1) and (2) can now be combined into one equation [11]:

$$h = \frac{2ft}{1+nt^2}, \quad (3)$$

where parameter n is equal to 0 for W-telescopes and n is equal to 1 for WS-telescopes. Equation (3) allows us to combine the surface equations of W- and WS-telescopes. Surface equation of the primary mirror can be expressed as [11]:

$$z = L + fk - \frac{h^2}{4fk} + C_z \frac{|k - (1 - nkt^2)|^{\frac{1-2nk}{1-nk}}}{|1+nt^2|^2}, \quad (4)$$

where $k = (s-L)/2f$ and C_z is an integration constant. Parameter s is the constant path length from the entrance aperture to the focal point. It can be easily calculated from the distances between the entrance aperture and the primary-secondary intersection point to the focus. Parameter C_z can be expressed in terms of system parameters as:

$$C_z = \frac{\left(L - fk + \frac{h_0^2}{2fk}\right) |1+nt_0^2|}{|k - (1 - nkt_0^2)|^{\frac{1-2nk}{1-nk}}}. \quad (5)$$

Parameter h_0 is the maximum entrance aperture radius and $t_0 = \tan(\alpha_0/2)$ where α_0 is the back angle of the secondary as shown in Figure 1. Equation of the secondary mirror can be written in terms of q and t as:

$$\frac{1+t^2}{q} = \frac{t^2}{fk} - \frac{1}{C_z k^2} |k - (1 - nk)t^2|^{\frac{1}{1-nk}}. \quad (6)$$

Equations (4) and (6) are valid for any combination of W- or WS-telescopes (or combination of parabolic primary mirror and hyperbolic or ellipsoidal secondary mirror if n parameter is selected to be 0). The surface equations seem complex, but they simplify comparison of W- and WS-telescopes since the surfaces are expressed as functions of the same parameters (L, f , and h_0).

3. RAY-TRACE AND DESIGN OF NESTED TELESCOPES

Our design tools are based on Equations (1) – (6). Nested telescopes have to be designed so that all the individual telescopes have the same focal length f_i . This means that the intersection points of the primary and secondary mirrors fall on a sphere with the radius f_i . WS-telescopes automatically meet this requirement ($f = f_i$). In order for W-telescopes to meet this requirement the f -parameter (axial radius of curvature of the principal surface) have to be slightly varied to force the distance from the surface intersection points to the focus to be constant f_i for all of the nested mirror pairs.

The radial heights of the nested mirrors have to be selected so that the adjacent surfaces do not obscure the rays from reaching the focal plane across the field-of-view of the telescope. A cross-section of a nested telescope is shown in Figure 2. Our design program checks that the rays emanating from the edge of the field-of-view hits the primary-secondary intersection point and clears the edge of the back corner of inner mirror on its way to the focal plane.

In the design program we select the physical lengths of the individual telescopes to be the same. There can be a predefined gap between the primary and secondary mirrors and one can select the thickness of the mirrors. The program starts stacking the primary and secondary mirrors from inside out. The nested pairs follow the shape of a surface which, in this case, is spherical. The design program iteratively finds the primary-secondary mirror intersection point of the outer pair of mirrors based on the surface data calculated for the inner pair of mirrors and then checks that the all the rays across the field-of-view are unobstructed by the inner surfaces.

Ray tracing tools are also based on Equations (1) - (6). Rays start at the entrance aperture. They are traced to the primary surface. The intersection point of the rays and surface are found iteratively. Rays are then traced to the secondary mirror. After iteratively finding the surface intersection point, the rays are traced to the focal plane. The program checks if the rays intersect the physical surface and are allowed to continue. Optical constants can be assigned to the surfaces to properly account for the reflection losses on the surfaces and calculate the telescope effective area. No mirror alignment, surface errors, or roughness are included in this study of nested telescopes.

Table 1. Dimensional requirements of the telescope

	Parameter value (mm)
Focal length f_i	5000.0
Minimum radial height of mirrors h_i	147.6
Maximum radial height of mirrors h_0	650.0
Axial length of primary and secondary L_p, L_s	100.0
Gap size of the primary and secondary c_p, c_s	10.0
Thickness of mirrors d	0.4

4. DESIGN DATA FOR SURVEY TELESCOPE

Optical design requirements for a survey telescope are listed in Table 1. Requirements are derived based on the fairing size of Taurus 3260 launch vehicle. Unobscured field-of-view of the telescope is 1.0-degree in diameter. The slope angle of the innermost mirror pair was selected to match the outer edge of the field-of-view. In other words, this mirror pair does not obscure the field-of-view. The mirror segments of the telescope will be fabricated using thermal slumping technologies or light-weight single crystal silicon technologies [12] developed at Goddard Space Flight Center. It is anticipated that separate primary and secondary mirror housings will be built and the housing units are divided into several mirror modules [13]. To allow room for the mirror housings, a small gap (20 mm) between primary and secondary surfaces is required. The gap should be as small as possible since the areas close to the surface intersection point provide the best imaging and minimizes the field curvature aberration terms.

4.1. Optical performance of single telescope

To compare W-, WS-, and MWS-designs one of the outer pairs was selected. The radial height of this pair at the primary-secondary intersection plane is 645.0 mm. Left column of Figure 3 shows ray density plots for

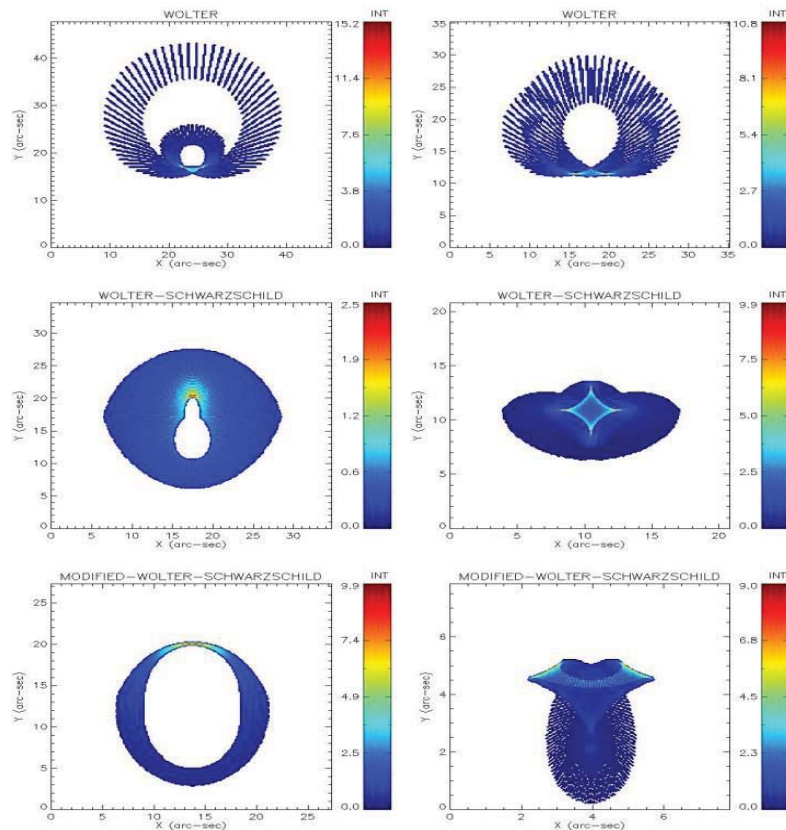


Figure 3. Ray density plots of W-, WS-, and MWS-telescopes plotted 0.5 degrees off-axis. Images in the left column are at the Gaussian focal plane and the images in the right column are at the best focal surface.

W-, WS-, and MWS-designs at the Gaussian focal plane and right column plots the ray density plots at the best focal surface 30.0 arc-min away from the optical axis. Double-circle of the W-design signifies the

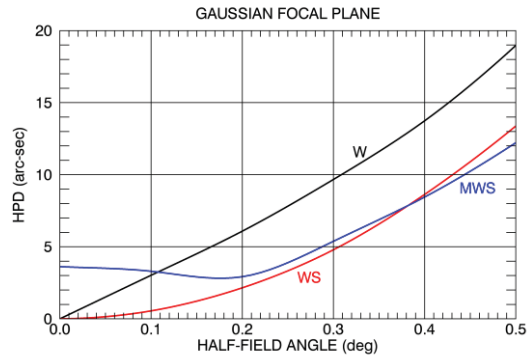


Figure 4. HPDs of W-, WS-, and MWS-telescopes at Gaussian focal plane.

presence of coma and field curvature. At the best focal surface the double-circles of coma have roughly the same diameter. Matching the circles minimizes the image size at the best focal surface. In case of WS-telescope, the image is much more symmetric. At the Gaussian focal plane the image is roughly circular with a hollow center. The outer parts of the image are oval mainly because large number of rays is vignetted at the secondary mirror. The rays are not equally distributed around the torus. At the best focus the image collapses to a more complex shape. Circular features coming from the field curvature are removed and the image has higher order azimuthal dependency indicating residual higher order aberrations. Note that the ring image of WS-telescope at the Gaussian focal plane is radially quite wide compared to its size. The width of the ring image can be narrowed by introducing a small amount of axial second order sag either on the primary mirror or on the secondary mirror. In the MWS-telescope 0.225 μm (peak-to-valley) axial sag is added to the primary mirror of WS-telescope. This process sharpens the ring image. At the best focal surface the image is significantly smaller than the image of the WS-telescope.

Figure 4 plots the HPD of W-, WS-, and MWS-telescopes as a function of half-field angle at the Gaussian focal plane. The HPD of W-design increases nearly linearly because the coma is a dominating aberration term. The HPD of WS-design has a larger second order component because the field curvature terms are the

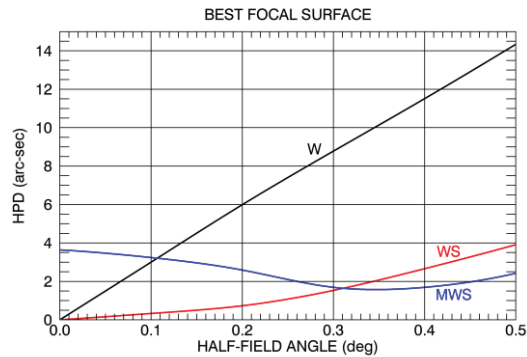


Figure 5. HPDs of W-, WS-, and MWS-telescopes at best focal surface.

dominating aberrations. In case of MWS-design, the perfect on-axis image is lost because of the added primary mirror axial sag. A slight decrease in HPD is seen at larger half-field angles.

In Figure 5 the HPDs of the three telescopes are plotted at the best focal surface up to 0.5 degrees. The HPD of the W-design is nearly linear since the effects of field curvature terms are minimized and coma is the dominating aberration term. The HPD of WS-design is reduced at small half-field angles and quadratic at larger half-field angles. The added sag of MWS-design increases the on-axis HPD to ~ 3.6 arc-sec. The HPD curve has a minimum at ~ 0.35 degrees. The added axial sag is radially focusing the rays to a significantly smaller central core. The WS-design is clearly superior to the MWS-design at small half-field angles. At half-field angles of 0.31 degrees and larger, the HPD of MWS-design is considerably smaller. The response of MWS-design is more uniform and the HPD can be below 4.0 arc-sec across the 1.0-degree field-of-view.

4.2. Optical performance of nested telescopes

Dimensional parameters of the nested telescope designs are listed in Table 1. The maximum number of mirror pairs that can be fitted to the design volume is 148. W- and WS-telescopes are designed so that the primary-secondary surface intersections follow the spherical principal surface of the WS-designs as illustrated in Figure 2. Iridium coatings on the optical surfaces are assumed. Optical constants published by Lawrence Berkeley Laboratory [14] were used to calculate reflection losses at the mirror surfaces.

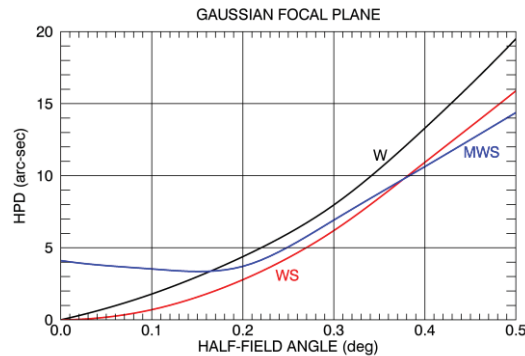


Figure 6. HPDs of nested W-, WS-, MWS-telescopes at Gaussian focal plane calculated at 1.0 KeV.

Figure 6 plots the HPD of W-, WS- and MWS- telescopes as a function of half-field angle calculated at 1.0 KeV. The HPDs are calculated from the ray tracing results only. No surface errors or assembly and alignment errors are assumed in the calculations. The HPD of MSW-design is significantly worse near the optical axis. The added second order axial sag of $0.255 \mu\text{m}$ on the primary mirror increases the HPD in this region. All of the mirror pairs of MWS-telescopes have the same on-axis HPD if the same amount of sag is added to the primary mirrors. In 0.4 - 0.5-degree range the HPD of MWS-design is slightly smaller. In this region the added sag compensate the radially symmetric image error inherent in WS-designs.

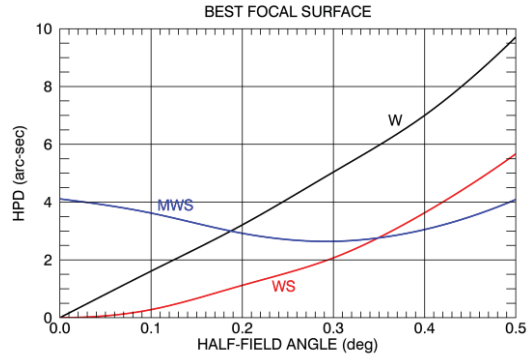


Figure 7. HPDs of nested W-, WS-, and MWS-telescopes at best focal surface calculated at 1.0 KeV.

In Figure 7 the HPDs of the designs are plotted at the best focal surface. The HPD of W-telescope is significantly larger because of the coma aberration in all of the individual telescopes. The HPD of WS-telescope is considerably smaller than the HPD of MWS-telescope up to about 0.3 degrees from the optical axis. At larger half-field angles the MWS-telescope is superior in terms of HPD. MWS-telescope delivers nearly uniform HPD across the field-of view. The HPD values range from 2.6 to 4.1 arc-sec.

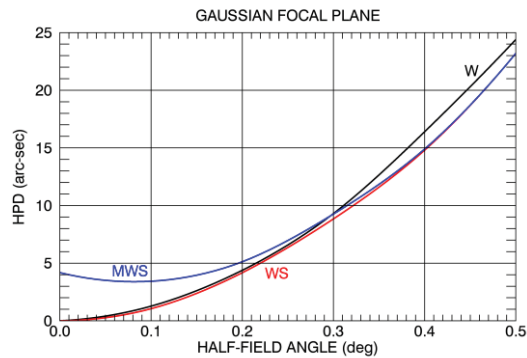


Figure 8. HPDs of nested W-, WS-, and MWS-telescopes at Gaussian focal plane calculated at 4.0 KeV.

In Figure 8 the HPDs of the telescopes are plotted at the Gaussian focal plane at 4.0 KeV. The HPD of nested W-telescope is slightly larger at large field angles. At small field angles W- and WS-designs are nearly identical, but MWS-telescope is significantly worse because of the added axial sag of the primary mirrors of MWS-design. At 4.0 KeV, field curvature aberration terms dominate since inner mirror pairs contribute more to the image. Because of this, WS-design is not significantly better than the W-design. The HPDs calculated at 4.0KeV and at the best focal surface are shown in Figure 9.

The HPD of WS-telescope is slightly better than the HPD of W-telescope. The HPD is under 10 arc-sec at the edge of 0.5-degree half-field. At 4.0 KeV, the inner mirror pairs contribute more to the shape and size of the image because reflectance losses are high on the outer mirrors. On the other hand, the geometric area of the outer mirrors is significantly larger increasing the effects of the outer shells to the shape and size of the image. Varying field curvature terms become the dominating aberration when more mirror pairs contribute more to the overall image. These aberration terms are significantly larger in inner mirror pairs. The HPD of

MWS-telescope is large in 0.0- to 0.25- degree range because of the added primary mirror axial sag. Increasing the sag would improve the HPD in 0.4- to 0.5-degree range but make the HPD worse in 0.0- to 0.1-degree range.

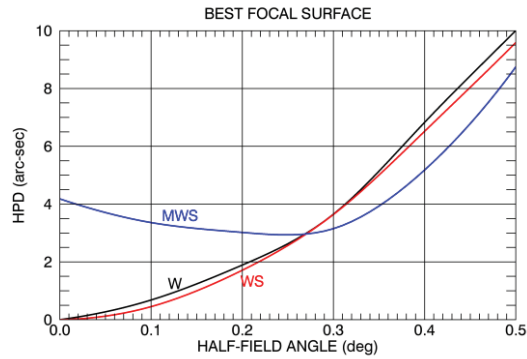


Figure 9. HPDs of nested W-, WS-, and MWS-telescopes at best focal surface calculated at 4.0 KeV.

Figure 10 plots the effective area of the telescope as a function of the half-field angle at 1.0 KeV and 4.0 KeV assuming no structural obscurations. These obscurations typically decrease the effective area 25% to 30% in a nested x-ray telescope. At 1.0 KeV, on-axis effective area is above 4000 cm². It drops nearly linearly to 2400 cm² towards the edge of the field-of-view. Vignetting is the driving factor which decreases the effective area and is the largest in the back part of the secondary mirrors. Increasing the axial length of the secondary mirrors would reduce the

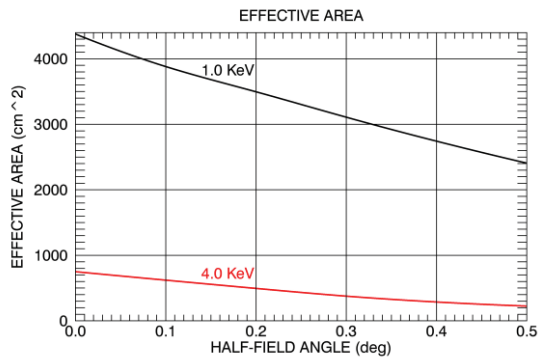


Figure 10. Effective area of the nested telescopes at 1.0 and 4.0 KeV.

vignetting, but longer secondary mirrors would reduce the backing density of the mirrors and this would lead to lowering of the effective area. The effective area is a factor of 5.8 lower at 4.0 KeV. The reflectance losses on the outer shells are the main factor behind the loss of the effective area at higher energies. To increase the effective area at 4.0 KeV, the telescope focal length would have to be longer. Replacing a single nested telescope with 3 nested and smaller telescopes could also boost the effective area up at higher energies.

Several detectors are needed to completely cover the best focal surface of the telescope. Reverse pyramid configuration with 4 detectors is one of the simplest options [15]. In Figure 11, the HPD is shown for the reverse pyramid configuration assuming that the tip of the pyramid is on-axis at the telescope focus, while the 0.5-degree off-axis (best focus) location is also on the detector diagonal axis. The HPDs calculated at 1.0 KeV are plotted for nested WS-telescope and MWS-telescope along the diagonal axis and edge of the detector. The HPD of the nested MWS-telescope is below 5 arc-sec along the diagonal direction and slightly over 5-arc-sec at the edge of the field along the edge of the detector. The HPD of nested WS-telescope is clearly larger at large field angles, but significantly better in 0.0 to 0.15-degree range.

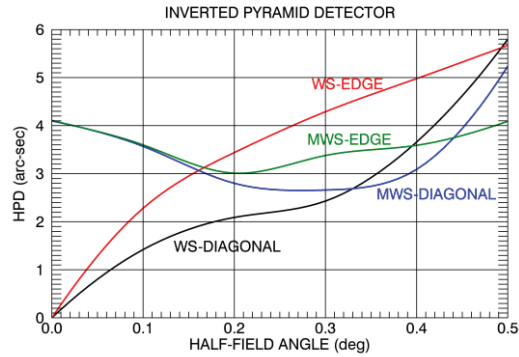


Figure 11. HPDs of nested WS- and MWS-telescopes assuming 4 detectors are placed in inverted pyramid configuration. The HPDs are calculated at 1.0 KeV.

5. CONCLUSIONS

General grazing incidence surface equations provide a simple platform to design complex nested x-ray telescopes. The equations are expressed as functions of convenient system parameters such as physical length, entrance aperture size, and focal length. The use of principal surface as the basic building block of a nested system, automatically guarantees that the focal lengths of the mirror pairs match. Comparison of Wolter and Wolter-Schwarzschild telescopes is straightforward because the same parameters are used to specify both designs. The drawback of the equations is their complexity and parametric form. The design tools have to find the dimensions of nested mirror pairs using iterative methods. Similarly, ray tracing would be harder with commercial ray tracing programs. Custom ray tracing tools provide a simpler alternative.

Wolter-Schwarzschild design can be used as a basis to generate and study new designs, since the Wolter-Schwarzschild telescope provides excellent on- and off-axis optical performance. The off-axis images are fairly symmetric because the telescope is free of coma. Small axial perturbations of the surfaces can be used to improve the telescope performance at the best focal surface. A simple sag adjustment of the primary mirrors in the Modified Wolter-Schwarzschild telescope can be used to improve the off-axis optical performance. This design provides more uniform optical performance across the field-of-view. No complex optimization analyses or optimization schemes are required.

Modest size and large field-of-view x-ray telescopes are feasible even when the focal length is fairly short. The nested telescope can be designed to provide overall image quality of about 5 arc-sec over 1-degree field of-view at x-ray energies around 1.0 KeV.

6. ACKNOWLEDGEMENTS

This work has been financially supported by the Next Generation X-Ray Optics Project at Goddard Space Flight Center in Greenbelt, Maryland.

REFERENCES

- [1] Hans Wolter, "Mirror systems with glancing incidence as image-producing optics for x-rays," *Ann. Phys.* **10**, 94 (1952).
- [2] Timo T. Saha, "Transverse ray aberrations for paraboloid-hyperboloid telescopes," *Appl. Opt.*, **24**, 1856-1863 (1985).
- [3] Timo T. Saha, "Aberration for grazing incidence telescopes," *Appl. Opt.*, **27**, 1492-1498 (1988).
- [4] R. C. Chase and L. P. VanSpeybroeck, "Wolter-Schwarzschild telescopes for x-ray astronomy," *Appl. Opt.*, **12**, 1042-1044 (1973).
- [5] James E. Harvey, Andrey Krywonos, Patrick L. Thompson, and Timo T. Saha, "Grazing incidence hyperboloid-hyperboloid designs for wide-field x-ray imaging applications," *Appl. Opt.*, **40**, 136-144 (2001).
- [6] Christopher J. Burrows, Richard Burg, and Riccardo Giacconi, "*Ap.J.*, **392**, 760-765 (1992).
- [7] Paolo Conconi, Sergio Campana, Gianpiero Tagliaferri, Giovanni Pareschi, Oberto Citterio, Vincenzo Cotroneo, Laure Proserpio, and Martha Civitani, "A wide field X-ray telescope for astronomical survey purposes: from theory to practice," *Mon. Not. R. Astron. Soc.*, **405**, 877-886 (2010).
- [8] Ronald F. Elsner, Stephen L. O'Dell, Brian D. Ramsey, and Martin C. Weiskopf, "Methods of optimizing x-ray optical prescriptions for wide-field applications," *Proc. of SPIE*, **7732**, 77322L-77322L-14 (2010).
- [9] Peter W. A. Roming, John C. Liechty, David H. Sohn, Jared R. Shoemaker, David N. Burrows, Gordon P. Garmire, "Markov chain Monte Carlo algorithms for optimizing grazing incidence optics for wide-field x-ray survey imaging," *Proc. of SPIE*, **4496**, 146-153 (2002).
- [10] Timo T. Saha, "Transverse ray aberrations of Wolter type 1 telescopes," *Proc. SPIE*, **640**, 10-19 (1986).
- [11] Timo T. Saha, "General surface equations for glancing incidence telescopes," *Appl. Opt.*, **26**, 658-663 (1987).
- [12] W.W. Zhang, M.P. Biskach, P.N. Blake, V.T. Bly, J.M. Carter, K.W. Chan, J.A. Gaskin, M. Hong, B.R. Hohl, W.D. Jones, J.J. Kolodziejczal, L.D. Kolos, J.R. Mazzarella, R.S. McClelland, K.P. McKeon, T.M. Miller, S.L. O'Dell, R.E. Riveros, T.T. Saha, M.J. Schofield, M.V. Sharpe, and H.C. Smith, "High resolution and high throughput x-ray optics for future astronomical missions," *Proc. SPIE*, **8861**, 88610N-1-88610N-13 (2013).
- [13] Ryan S. McClelland, Michael P. Biskach, Kai-Wing Chan, Rebecca A. Espina, Bruce R. Hohl, Elizabeth A. Matson, Timo T. Saha, William W. Zhang, "Design, construction, and testing of lightweight x-ray mirror modules," *Proc. of SPIE*, **8861**, 88610O-1-88610O-13 (2013).

[14] http://henke.lbl.gov/optical_constants/

[15] Ronald F. Elsner, Stephen L. O'Dell, Brian D. Ramsey, and Martin C. Weisskopf, "Mathematical formalism for designing wide-field x-ray telescopes: mirror nodal positions and detector tilts," *Proc. of SPIE*, **8147**, 814712-1-814712-15 (2011).